# Role of Generated Free Radicals in Synthesis of Amorphous Hydrogenated Boron Carbide from *ortho*-Carborane using Argon Bombardment: A ReaxFF Molecular Dynamics Study

Nirmal Baishnab<sup>1</sup>, Rajan Khadka<sup>1</sup>, Michelle M. Paquette<sup>2</sup>, Paul Rulis<sup>2</sup>, Nathan A. Oyler<sup>3</sup>, Jinwoo Hwang<sup>4</sup>, Ridwan Sakidja<sup>1</sup>

- <sup>1</sup> Department of Physics, Astronomy, and Materials Science, Missouri State University, Springfield, MO 65897
- <sup>2</sup> Department of Physics and Astronomy, University of Missouri-Kansas City, Kansas City, Missouri 64110
- <sup>3</sup> Department of Chemistry, University of Missouri-Kansas City, Kansas City, Missouri 64110
- <sup>4</sup> Department of Materials Science & Engineering, The Ohio State University, Columbus, Ohio 43210,

## **Abstract**

In this study, we modeled and analyzed a critical aspect of the synthesis process for a- $B_x$ C: $H_y$  i.e. the argon bombardment from the *ortho*-carborane precursor. Utilizing the reactive molecular dynamics simulations, we identified and evaluated the formation of free radicals as a result of ion bombardment. We found that increasing kinetic energy of ions releases an increasing amount of hydrogen. Thus, hydrogen content in the product can be tuned by varying the ion energy. Overall, our approach allows for a better understanding of the mechanism of Ar bombardment and the role of radical species toward the formation of ortho-carborane network.

Keywords: Molecular Dynamics, ReaxFF, Boron Carbide, Amorphous, Ceramics, Argon Bombardment

## 1. Introduction

High strength ceramics such as boron carbide and silicon carbide can potentially be used for a wide range of structural applications. These ceramics in general have a higher mechanical strength than typical metals.[1–6] Boron carbide, for example, is the third hardest material in nature following diamond and cubic boron nitride.[1] Its combined high hardness and very low density offer an attractive materials choice, especially when the strength to weight ratio is taken into consideration. In addition, it is thermally stable with a very high melting temperature, above 2500 K. Combined with its high abrasion resistance[1], the thermal stability and strength of boron carbide amount to an attractive set of physical properties well-suited for body armor components and abrasives. Since boron-10 has a high cross-section for neutron absorption, boron carbide is also an important

material for nuclear reactors[7,8] and neutron detection[9,10]. Lastly, within the semiconductor industry, thin-film boron carbide can also be used for insulating low-dielectric-constant (low-*k*) intra/interlayer dielectrics [11], patterning materials for semiconductor devices, optical films, and other specialized electronic applications.[12–15]

There have been a wide variety of growth techniques developed to produce boron-carbide-based solids[1,2] including hot pressing and pressureless sintering.[16–18]. These synthesis routes generally require high temperatures and have been used primarily to produce boron carbide for structural/engineering applications such as armor and abrasives. However, these bulk processing techniques can not be easily integrated with semiconductor device processing and oftentimes do not yield desirable electronic properties.[19,20]. Alternatively, chemical vapor deposition (CVD) or physical vapor deposition (PVD) techniques have been found to be

xxxx-xxxx/xx/xxxxxx 1 © xxxx IOP Publishing Ltd

quite useful in generating B<sub>x</sub>C thin films with mechanical, thermal, and chemical properties comparable to those of the bulk materials. Furthermore, their electronic properties can be tuned and enhanced.[21-25] In particular, thin films derived from ortho-carborane (o-C<sub>2</sub>B<sub>10</sub>H<sub>12</sub>) using a plasma-enhanced chemical vapor deposition (PECVD) technique have been demonstrated to possess promising properties for a variety of device applications.[26-31] This fabrication approach produces an amorphous hydrogenated boron carbide (a-B<sub>x</sub>C:H<sub>y</sub>) variant, which is quite novel in the field of electronic materials. The electronic, optical, chemical, and mechanical properties of these films have been extensively investigated, and in particular the influence of hydrogen on these properties.[32] However, it is still an open question as to which types of free radicals form during the PECVD process as well as how the ionic bombardment contributes to the overall formation of ortho-carborane aggregates leading to the formation of the thin films and the overall hydrogen retained in the product. In this study, we attempt to gain a more fundamental insight into this process through a systematic investigation of the impact of argon bombardment on orthocarborane in the gaseous phase.

# 2. Computational approach

Since a single molecule of orthocarborane is already comprised of 24 atoms,[32,33] modeling an assembly of hundreds of these molecules would be quite difficult if we were to utilize a quantum mechanical (QM) approach.[34–37] The maximum number of atoms that can be modeled by means of ab-initio calculations is limited to only a few hundred atoms. In order to overcome this limitation while maintaining nearly the same level of accuracy as achieved by QM calculations, we thus opted instead to perform reactive molecular dynamics (MD) simulations by using a carefully parameterized empirical ReaxFF reactive force method.[38,39] The reactive molecular dynamics simulation can significantly reduce simulation time by several orders of magnitude and is capable of defining continuous bond formation/breaking events during the simulations by monitoring the bond orders and energies of all of the pairs within the simulation.[38–43] For this study, we have used the ReaxFF force field developed by An et al,[44] for which parameters have been carefully parametrized to model crystalline and amorphous materials made of boron, carbon, and hydrogen atoms. In An et al,[44] though QM interactions of two C<sub>2</sub>B<sub>10</sub>H<sub>12</sub> molecules (icosahedral ortho-carborane or one of its isomers) were included in the ReaxFF fitting parameters, the application of that force field is shown mainly boron-carbide-based material. Therefore, proceeding, we determined the applicability of ReaxFF by comparing some results as calculated by QM and ReaxFF. This includes BH and CH bond dissociation energies in the ortho-carborane molecule as well as the total energies of different common species of boron, carbon, and hydrogen relevant to our study.

To simulate the Ar ion bombardments, Lennard Jones (LJ) potentials have been commonly used, as during bombardment the consideration is mostly the transfer of kinetic energy from high-energy ions to the bombarded species.[45,46] For our studies, we have also used the LJ potential to represent the pair interactions between Ar with the rest of the species. Each of the two LJ interaction parameters ( $\sigma$ , which is correlated to equilibrium distance of paired atoms and  $\varepsilon$ , which is associated with the minimum energy) for argon-argon and argon-carbon were obtained from Norio Inui et al.[46] They modeled the dynamic impacts of argon clusters onto a free-standing graphene monolayer. The optimized LJ parameters from their study are:  $\sigma_{Ar-Ar} = 3.4$  Å,  $\varepsilon_{Ar-Ar} = 0.23983$  Kcal/mol,  $\sigma_{Ar-C} =$ 3.385 Å, and  $\varepsilon_{Ar-C} = 0.115303$  Kcal/mol. Boron-boron LJ parameters were obtained from Baowan et al,[47] a study on boron nitride (BN) and carbon boron nitride (CBN) nanocones. Finally, hydrogen LJ parameters were obtained from thermophysical studies of H<sub>2</sub>O and argon plasma. [48] the Lorentz-Berthelot combination, [49,50] we calculated the LJ parameters, namely  $\sigma_{Ar-B} = 3.4265 \text{ Å}$ ,  $\varepsilon_{Ar-B} =$ 0.150885 Kcal/mol,  $\sigma_{Ar-H} = 3.054$  Å, and  $\varepsilon_{Ar-H} = 0.13283$ Kcal/mol. According to the Lorentz-Berthelot combination rule, we can define  $\sigma_{1-2} = (\sigma_{1-1} + \sigma_{2-2})/2$  and  $\varepsilon_{12} = (\varepsilon_1 \varepsilon_2)^{1/2}$ . For the MD simulations, we used the highly efficient Large-scale Atomic/Molecular Massively Parallel Simulator (LAMMPS) MD code,[51] which was developed by Sandia National Laboratories and has been successfully used to perform classical MD events on a wide range of materials.[52-58]

## 3. Simulation details

# 3.1 Quantum mechanics calculations

As previously mentioned, for determining the applicability of the force field, we calculated the bond dissociation energies of BH and CH in the ortho-carborane molecule and total energies of different relevant species (both chemically active and stable) of B, C, and H such as ortho-carborane, borane, and diborane using both ReaxFF and QM calculations. The QM calculations were performed using the commercial Vienna Ab-initio Simulation Package (VASP).[59] Plane wave basis set and projector-augmented wave (PAW) based pseudo-potentials are implemented in the software.[59-62] The ultra-soft pseudopotential with the Perdew Burke Ernzerhof (PBE) version of the generalized gradient approximation (GGA) exchange-correlation functional of DFT is adopted in substitution of core nuclei and valence electron exchange-correlation term calculation. We used the Monkhorst–Pack[63] scheme to create the k-space matrix. The plane wave basis set energy cut off was set to 520 eVm, and the tetrahedron method with Blöchl corrections smearing was selected with sigma value 0.2.

# 3.2 Argon bombardment of ortho-carborane molecules

Our primary focus was to study the impact of argon bombardment on ortho-carborane in the gaseous phase. In order to create the gaseous mixture, 1000 ortho-carborane molecules and 25 Ar atoms were packed into a small cubic cell with a unit cell of 102 Å. PACKMOL code[64] was used to randomly populate these species within the box. We also sampled one larger simulation box (8× the size of the initial box) comprising 8000 ortho-carborane molecules and 200 Ar atoms to provide better statistics on the gaseous products during the bombardment processes. The kinetic energy of the argon atoms was varied from 100 to 600 eV in 50 eV increments. For our interatomic potentials, 50 eV argon energy is not enough to break ortho-carborane, while 600 eV is set as the upper limit of the theoretical studies of argon energy distribution similar to previous studies.[65,66] The direction of the high-kinetic-energy argon atoms was initially kept random in order to mimic the interaction in the gaseous phase. The bombardment was performed for 5 ps with 0.05 fs time steps using the constant volume and energy simulation method (NVE ensemble). We chose to adopt a relatively small time step[67] due to the high kinetic energy. The whole simulation cell was subsequently equilibrated at 300 K using the constant volume and temperature method (NVT) for 100 ps with 0.25 fs time steps. We imposed periodic boundary conditions in all axes. In the NVT ensembles, the temperature of the box was controlled via a Nose-Hoover thermostat.

In order to analyze the impact of argon bombardment, we started the analysis by undertaking a pair distribution function (PDF) analysis of different atomic pairs, namely BH, HH, and CH. We carried out the time evolution of the species count of those that were created at the initiation of the NVE simulation. Different cutoff distances were used in the analysis at different cooling stages of the simulation to accurately count the number of species, as the interatomic distance naturally varies with temperature.

We found tens of different types of radicals and small clusters during bombardment, including both chemically stable and unstable species. We recorded the statistics of the most common species every 0.5 fs for the first 5 ps of the Ar bombardment. The data was then used to quantify correlations among these. To calculate the correlations we used the machine learning software WEKA [68]. WEKA is an open-source code embedded with several machine learning algorithms. It has been widely used for data mining purposes. [69–72] It also features a collection of mathematical approaches such as linear regression or multilayer perception to study correlations. We have used the linear regression method for our study.

## 4. Results & Discussion

# 4.1 ReaxFF verification

The reactive force field we opted to use has been previously parameterized through QM calculations to reproduce structure, energy, and reaction barriers.[44] It has been successfully used to analyze the mechanisms of brittle failure of non-hydrogenated crystalline and amorphous boron carbide. Here, we initially begin by testing the applicability of the ReaxFF potential in the analysis of ortho-carborane, a hydrogenated BC-based precursor. Figure 1 shows the bond dissociation energy curves of BH (a) and CH (b) from ReaxFF and DFT calculations. For both bonds the distances were taken up to 5 Å. Figure 1 indicates that the ReaxFF data are in good agreement with the DFT results. Additionally, Table 1 compares the formation energy of different species using DFT and ReaxFF. While Table 1 is far from complete, it shows that ReaxFF yields results fairly similar to those produced by DFT. However, we do notice that the formation of the B<sub>2</sub>H<sub>6</sub> dimer is much more favorable in the case of DFT. From the DFT calculations, the energy of formation,  $\Delta H$ , of the reaction  $2BH_3 \rightarrow B_2H_6$  is calculated as -50.54 Kcal/mol, whereas for ReaxFF it is calculated as -11.58 Kcal/mol. The calculated DFT value of -50.54 Kcal/mol is slightly higher than the experimental value of -41.50 Kcal/mol.[73] This indicates that ReaxFF would have underestimated the stability of B<sub>2</sub>H<sub>6</sub>, and indeed this was observed in our MD simulation results as discussed in section 4.2.2. Nevertheless, since both BH<sub>3</sub> and B<sub>2</sub>H<sub>6</sub> are gaseous products[74,75] with the same relative hydrogen percentage, this should have a minimal impact on the primary focus of our analysis, which is the hydrogen content in the solid clusters.

Table 1. Total energy in Kcal/mol of different molecules found during argon bombardment of *ortho*-carborane as calculated by DFT and ReaxFF.

Species	DFT	ReaxFF
$C_2B_{10}H_{12}$	-2986.766	-2730.7208
$H_2$	- 156.1239	-108.26742
BH <sub>3</sub>	-366.4476	-329.2619
CH <sub>4</sub>	-554.41	-428.45397
$B_2H_4$	-578.1819	-523.73947
$B_2H_6$	-783.496	-670.1018

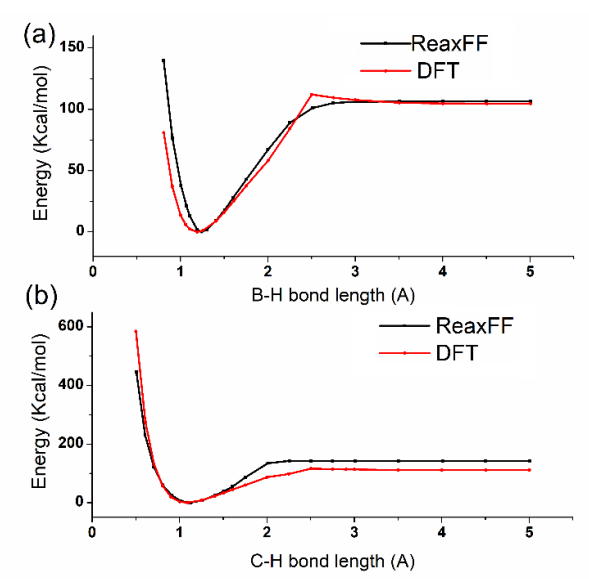


Figure 1. Bond dissociation energy using ReaxFF and DFT for (a) BH and (b) CH bonds.

In additional testing, we demonstrated that ReaxFF was able to produce a stable structure for the solid crystalline phase of *ortho*-carborane. As shown in Figure 2, we were able to reproduce the FCC crystal structure of *ortho*-carborane at room temperature with a unit cell dimension of ~10.9 Å, which is in good agreement with the experimental findings.[76]

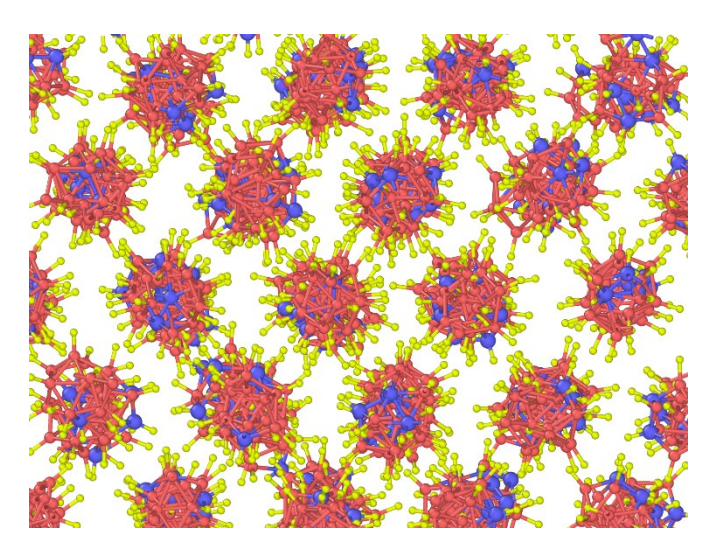


Figure 2. Crystal structure of *ortho*-carborane obtained at room temperature using ReaxFF. The red, blue, and yellow colored atoms represent boron, carbon, and hydrogen respectively.

# 4.2 Argon bombardment

As illustrated in Figure 3, which represents a trajectory of the *ortho*-carborane molecule almost immediately after its collision with energetic argon, the kinetic energy from Ar is transferred into the molecule and as a consequence, we observe the formation of a variety of species. In Figure 3, for

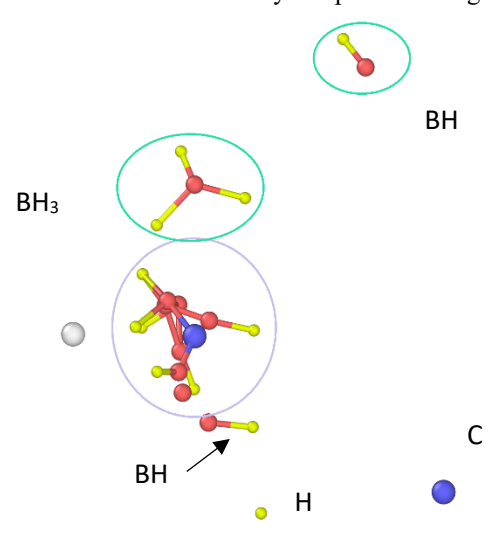


Figure 3. Snapshot after about 60 fs of the collision between a single *ortho*-carborane molecule and a 190 eV Ar atom.

example, we observe the formation of a cluster consisting of seven B atoms, one C atom, and six H atoms, a BH<sub>3</sub> molecule, BH radicals, and isolated carbon and hydrogen radicals.

## 4.2.1 Pair distribution function analysis

In order to analyze the formation of species during argon bombardment in greater detail, we took the structure data of the simulation cell at different times and performed a pair distribution function (PDF) analysis. In Figure 4, we present the PDF analysis of BH pairs at different times of the simulation with 25 argon atoms of 600 eV kinetic energy. The dominant peaks at 0 ps are from the different orders of the nearest neighbors from the initial ortho-carborane molecule. Due to the presence of carbon atoms in the molecule, the structure is slightly distorted from a regularly shaped B-only icosahedron because of the assymetry in bond length generated by the C atoms. In addition, there are some slight variations in the BH and CH bond lengths at the initial setting prior to bombardment noted in Figure 4. Because of Ar bombardments, some of the icosahedral structures would fracture causing a wider range of interatomic distances for each pair as evident from the gradual attenuation/broadening of peaks, also seen in Figure 4. PDF analysis of HH pairs further supports this observation as we can again see the gradual diminishing of initially sharp peaks, as shown in Figure 5. These initial peaks originated from adjacent H atoms within ideal icosahedral structures, initially bound to either B or C atoms within the ortho-carborane. Within the initial crystalline structure, no H–H bonds were present, as shown in Figure 2. After argon bombardment, we observe two newly formed peaks at ~0.75 Å and ~2.1 Å, which can be attributed

to the formation of hydrogen molecules and BH<sub>3</sub> molecules, respectively.[77]. At the end of the NVE simulations, the temperature remained high and thus the PDF remain fairly diffused. However, after quenching the structure to room temperature by means of NPT canonical ensembles, we would then observe one dominant and fairly sharp peak below 2 Å indicating the formation of stable hydrogen molecules.

## 4.2.2 Species calculation

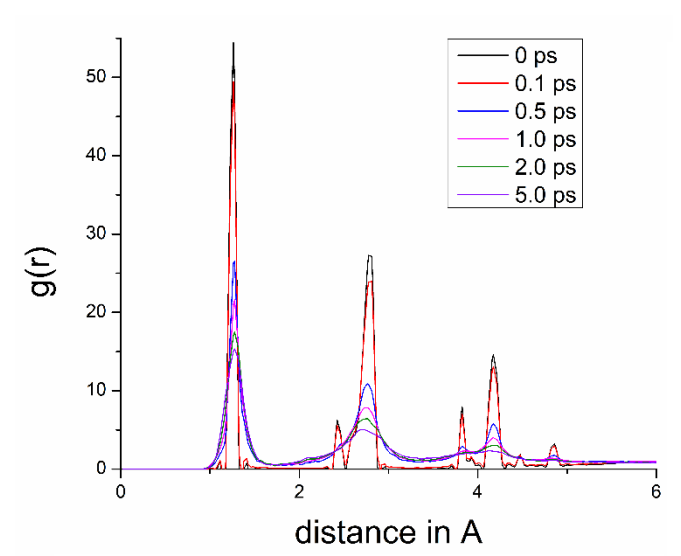


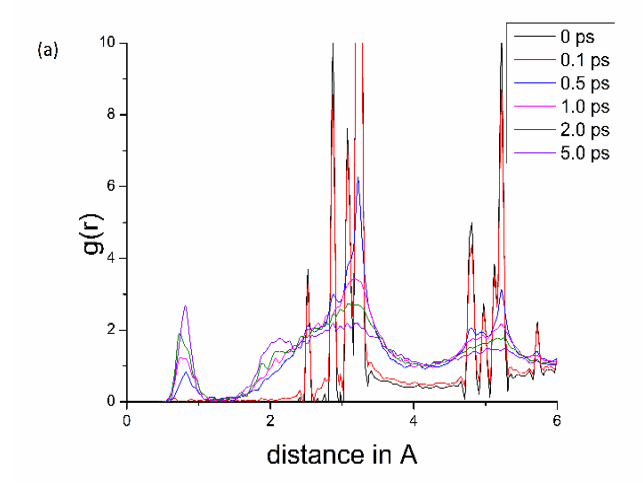
Figure 4. PDF analysis of BH pair for 600 eVAr bombardment at different time steps.

We showed earlier that, when a high-energy argon atom collides with an *ortho*-carborane molecule, different kinds of species and clusters form. Here we quantitatively and qualitatively investigate these species. We will refer to each simulation by the kinetic energy of the argon atoms set at the beginning of the bombardment. For instance, the particular simulation for which the bombardment was started with assigning 400 eV kinetic energy to all of the 25 argon atoms will be referred to as a 400 eV simulation.

We have calculated bond order values to determine the presence of chemical bonds. The bond order calculations were performed using the built-in method of ReaxFF in LAMMPS (reax/c/species). In the beginning, we put 1000 *ortho*-carborane molecules in all of our simulations.

Figure 6 shows the most common species found including small clusters, free radicals, *ortho*-carborane, and bigger clusters at different times for the 600 eV simulation. With the the use of small clusters, the dynamics involving the statistics of the main species can be assessed. It does not however necessarily capture the statistical dynamics of the smaller species population. Using 600 eV as the highest kinetic energy we have used for argon, we found a considerable amount of hydrogen generated in the simulation cell after 1 ps of the simulation time. Figure 6 indicates that most of the hydrogen was produced within 1 ps and it grew slowly but consistently

over time. More than 300 molecules of hydrogen (more than 5% of the total hydrogen) were found after 5 ps of bombardment and the quantity was unchanged after equilibration at room temperature. Initially, lots of H radicals were formed, which are chemically very active and unstable. The number of H atoms decreased drastically and almost disappeared by the end of the simulation. This can be explained by the fact that two hydrogen atoms easily react to produce H<sub>2</sub> molecules. Other active BH and BH<sub>2</sub> free radicals were found to form after 1 ps of simulation due to the fragmentation of ortho-carborane molecules by the energetic Ar impact. In the experimental Ar plasma environment, free radicals such as H, BH, CH, and CH2 have been reported as the main products during the plasma compositional analysis of PECVD with trimethylboron[78] and triethylboron[79] precursors. In our modelling process using *ortho*-carborane, the dominant BH, BH<sub>2</sub>, CH, and atomic H species are similarly found to be formed right after argon ion impact. The BH and BH<sub>2</sub> species, however, are found to subsequently disappear after equilibration, which can be explained by the



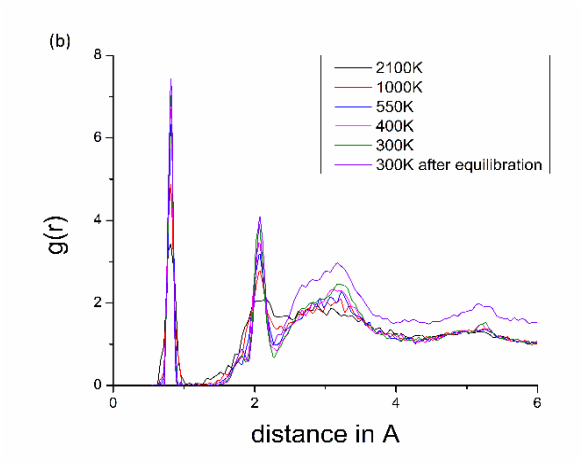


Figure 5. PDF analysis of HH pair for 600 eV: (a) during NVE, (b) NVT.

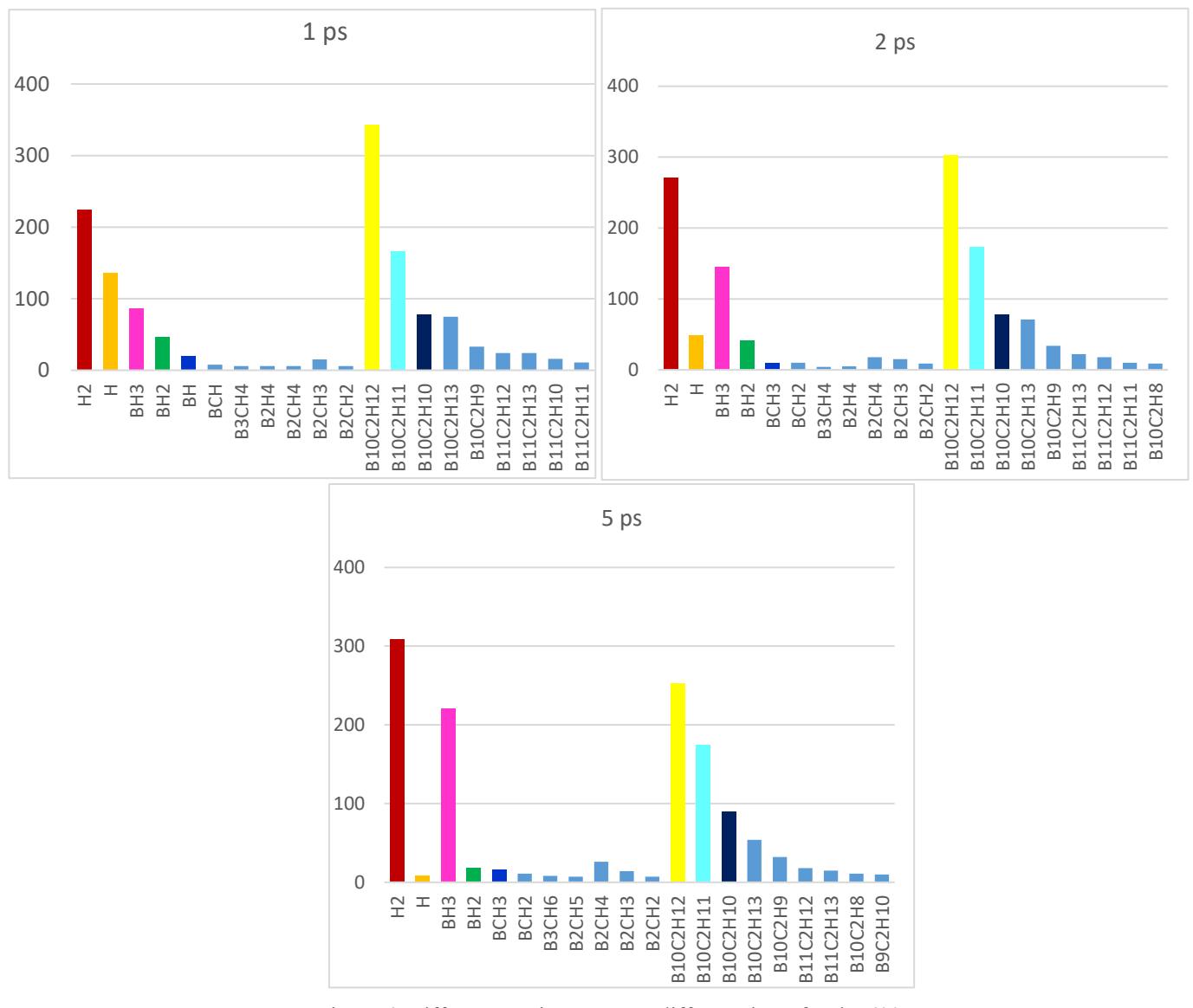


Figure 6. Different species counts at different times for the 600 eV simulation.

fact that some of them readily form bonds with H radicals and transform into BH3 gas. This is consistent with a previous Ar bombardment study, [80] which concluded that the formation of BH3 gas was the favorable pathway for PECVD chemistry in both Ar and H<sub>2</sub> atmospheres with triethylboron as precursor. The formation of these gaseous species could be the possible reason for the lack of any extraicosahedral B environments detected in the PECVD experimentally derived thin films [81]. This may imply that while favorable subsequent reactions involving BH, BH<sub>2</sub> and then BH<sub>3</sub> gaseous species should indeed readily take place in the presence of the H radicals, these remaining volatile species will likely be removed from the thin films. Thus, the resulting thin film would be slighly depleted from B which was quite consistent woth the experimental finding. However, we should however note that there have been reports of both B and C types of

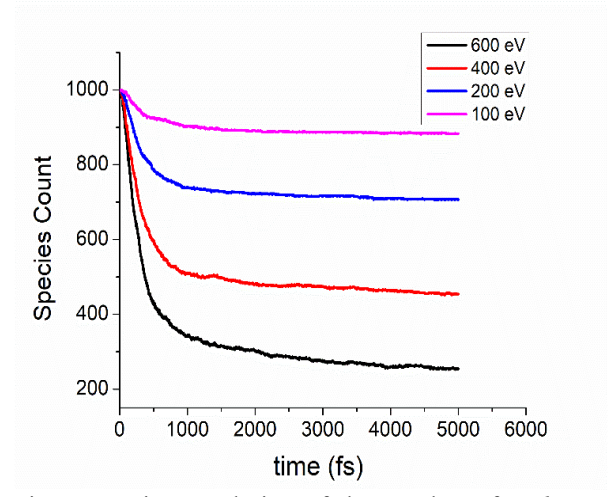


Figure 7. Time evolution of the number of *ortho*-carborane molecules for different argon ion energies.

extraicosahderal environment found in films derived from *ortho*-carborane precursors subject to different processing environments [82][83].

The trend for the amount of BH<sub>3</sub> molecules was found to be very similar to that of the H<sub>2</sub> molecules, whereas the variation in the concentration of BH and BH<sub>2</sub> species tends to follow the trend of the variation in the H concentration. Metastable species like BCH, B<sub>2</sub>CH<sub>2</sub>, B<sub>3</sub>CH<sub>3</sub>, B<sub>2</sub>CH<sub>4</sub>, B<sub>3</sub>CH<sub>4</sub>, and others are found in small numbers. Most likely, clusters like BCH and BCH<sub>2</sub> were formed from direct collisions

with H radicals in the vicinity of the surrounding *ortho*-carborane molecules.

Figure 7 shows that for the 100 eV simulation, around 10% of the *ortho*-carborane molecules were fragmented after 5 ps, whereas more than 800, i.e. 80%, were fragmented for the 600 eV simulation. Figure 8 shows the time evolution of different species created for different simulation energies. For the 600 eV simulation, the highest number of BH and CH free radicals was observed within 200–300 fs. BH was found to be the most common type of free radical at the beginning, aside from H.

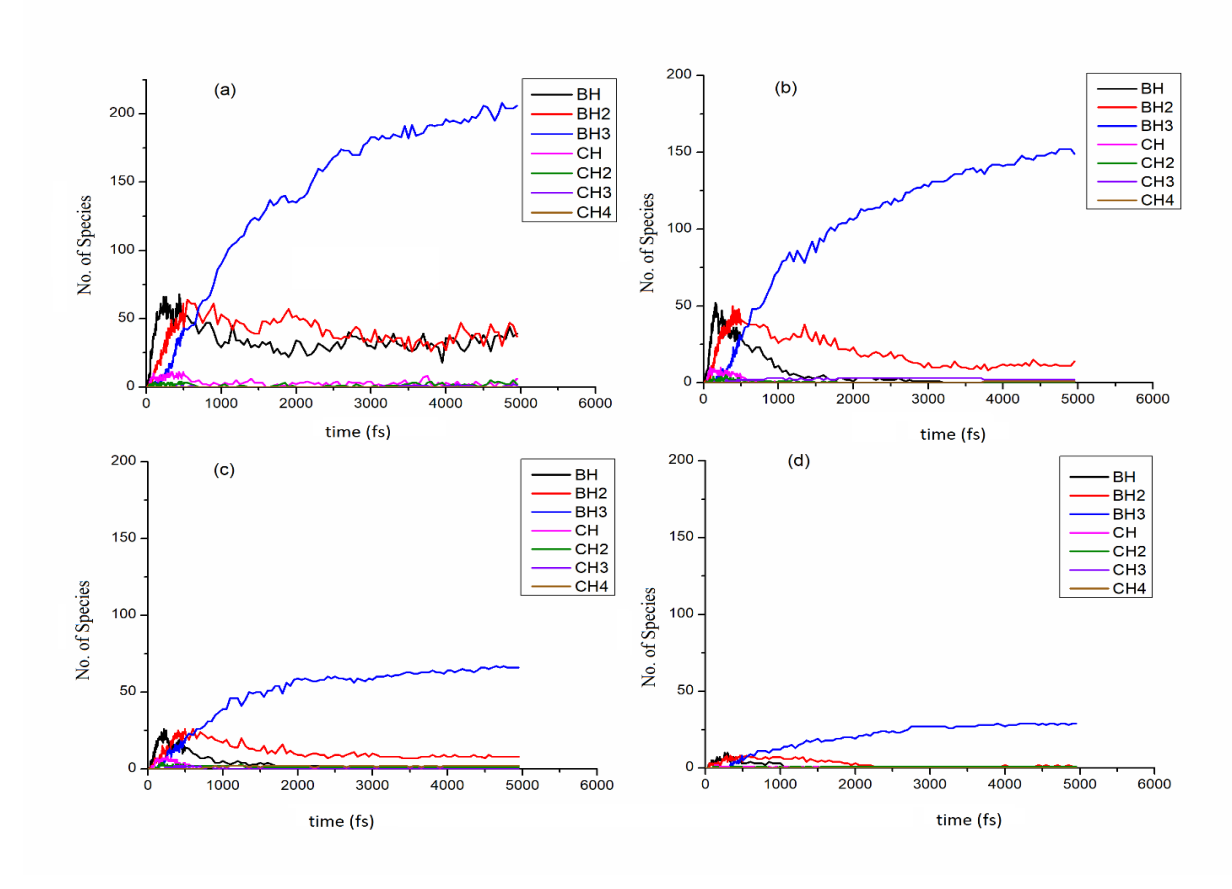


Figure 8. Time evolution of the number of different species for different argon ion energies: (a) 600 eV, (b) 400 eV, (c) 200 eV, (d) 100 eV.

between Ar and orthocarborane. Others may have been created from isolated B, C, and H atoms/radicals in the vicinity of BCH and BCH<sub>2</sub>. In analyzing the trend in behavior of the bigger clusters, we observed that the number of *ortho*-carborane molecules dropped to around 33% of the initial count within 1 ps. Deprotonation of the *ortho*-carborane molecules was observed with the evolution of icosahedral clusters including B<sub>10</sub>C<sub>2</sub>H<sub>11</sub>, B<sub>10</sub>C<sub>2</sub>H<sub>10</sub>, and B<sub>10</sub>C<sub>2</sub>H<sub>9</sub>. The formation of these partially dehydrogenated species of *ortho*-carborane is in good agreement with the PECVD radicals formed during the Ar plasma environment [84]. In addition, some of the free radicals generated by bombardments such as B, BH, C, and CH are relatively unstable and thus readily react

After peaking at around  $\sim 200-300$  fs, the quantity decreased dramatically, presumably due to its reaction with the surrounding species. The amount of BH<sub>2</sub> radicals, which also initially peaked, shows a similar decrease with time, albeit slightly more gradual. Presumably, this is due to the difficulty, over time, to find remaining H radicals to transition to BH<sub>3</sub>.In general, the amount of CH<sub>n</sub> is low. This may indicate the difficulty in stabilizing CH<sub>n</sub> species relative to their BH<sub>n</sub> counterparts. In addition, we observed smaller amounts of CH<sub>3</sub> and CH<sub>4</sub> species relative to CH and CH<sub>2</sub>. Presumably, this is due to the majority amount of C-related radicals generated by bombardment have been interconnected with the surrounding *ortho*-carborane molecules. This may also be due to the

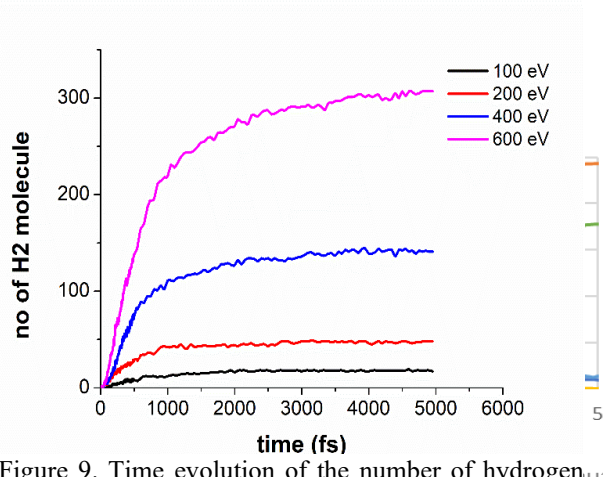
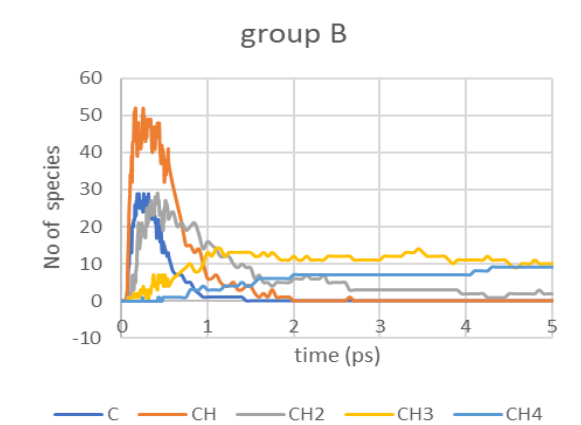
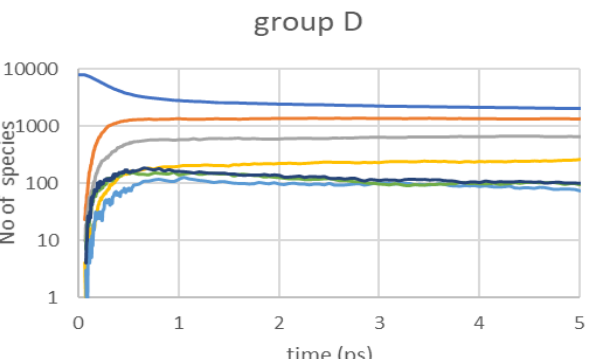


Figure 9. Time evolution of the number of hydrogen, H3 molecules for different argon ion energies.

group C

bombardment, we did not observe the proposed chemical reaction.





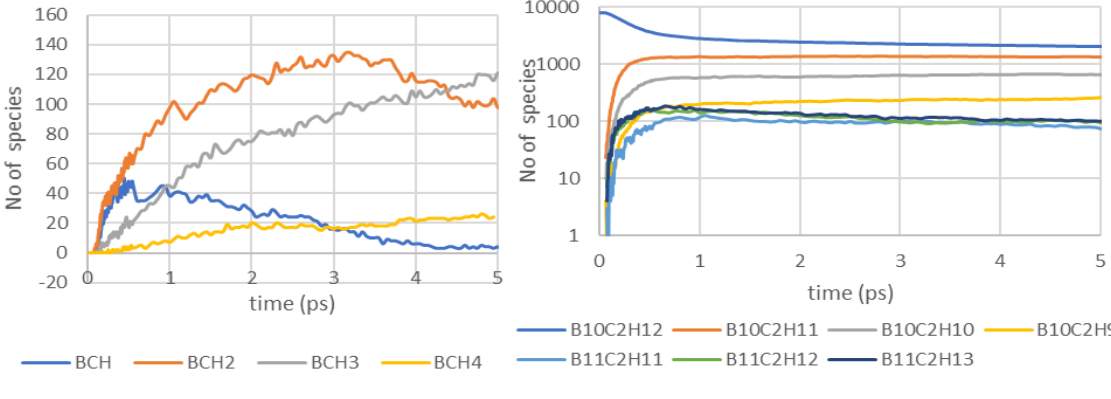


Figure 10. Time evolution of different categorized species for 600 eV argon energy.

relatively smaller amount of CH (relative to BH), limiting the possibily for further reactions with H radicals. Our finding of C atoms in extra-icosahedral environment in the form of CH<sub>2</sub> and CH3 has been reported in a number of PECVD film depositions.[81,85-88] BH<sub>3</sub> gas molecules, on the other hand, were highest among all these species at the end of the bombardment simulations and consistently increased over time. This can be understood by the fact that BH<sub>3</sub> is a relatively stable molecule, forming a 2D planar structure.[77] Without a sufficient external kinetic disturbance, these molecules should remain stable once formed. In Figure 9, the amount of hydrogen produced over time is shown. The trend is similar with BH<sub>3</sub> since H<sub>2</sub> is also a stable molecule and, once formed, will remain chemically stable. Our observation of the formation of stable BH3 and H2 is in agreement with the reaction using the single solid triethylboron.[80] Another previous study by Imam et. al.[79] showed the dominant formation of BH and H<sub>2</sub> in the plasma. This was proposed to result from the dehydrogenation of BH<sub>3</sub> in the presence of excess H radicals. In our MD simulation study, since the H radicals have been primarily consumed by H<sub>2</sub> gas formation at the early stage of the simulated Ar

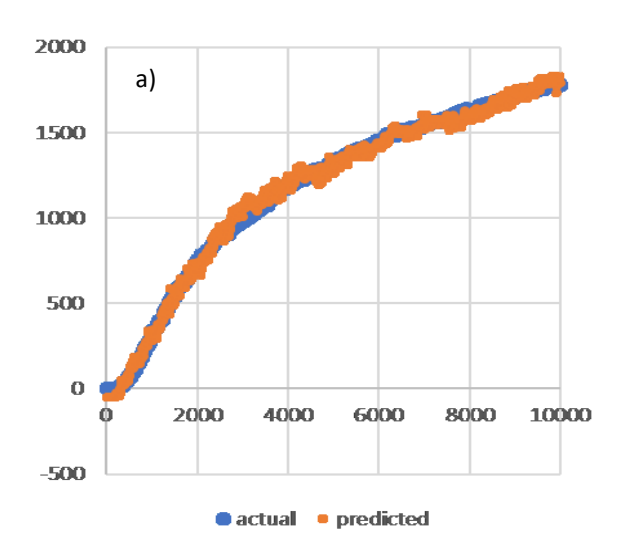
Overall, the correlation between the initial kinetic energy of argon and the number of species generated can be quantitatively evaluated through our MD simulations. In addition, the hydrogen content in the formed clusters is in good agreement with previous studies.[32,81,89]

### 4.2.3 Species correlation: regression analysis

Based off MD simulation results using 1000 orthocarborane and 25 Ar atoms, we were able to identify the main species formed and evolved during the processes. To improve the statistics, we made a new simulation cell with 8000 orthocarborane molecules and 200 argon atoms. The density of the gaseous mixture (i.e., the ratio of ortho-carborane to Ar) was kept the same as before. For the sake of representation, we categorized the important species in four different groups based on the combination of types of atoms. Figure 10 shows the time evolution of these groups of species for 600 eV argon energy. The outcomes from this new structure are consistent with those produced by smaller scale simulations. The number of active species like B, BH, H, C, CH, CH<sub>2</sub>, and BCH were grown at the initiation of the ion bombardment. However, their number declined quickly as they started creating bonds

with other species and clusters in their vicinity. Less active and metastable species like  $BH_2$ ,  $CH_3$ ,  $BCH_2$  declined comparatively slowly. Gradual protonation showed the following pattern:  $B > BH > BH_2 > BH_3$ ,  $C > CH > CH_2 > CH_3 > CH_4$ ,  $BCH > BCH_2 > BCH_3 > BCH_4$  and so on. From group D the trend of originated clusters from *ortho*-carborane is observed. It should be noted that the Y axis for group D is in log scale. Mostly, orthocarborane deprotonated and generated clusters such as  $B_{10}C_2H_{11}$ ,  $B_{10}C_2H_{10}$ , and  $B_{10}C_2H_9$ .

In Figure 11a and 11b the actual and predicted data of BH<sub>3</sub>



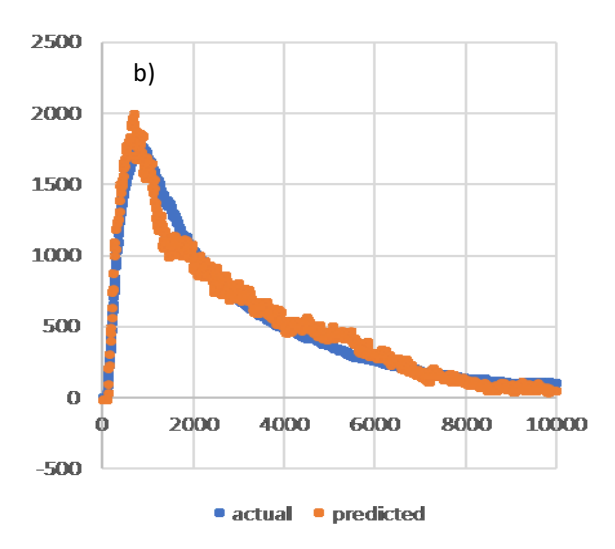


Figure 11. Correlation between the time of evolution of the number of a) BH<sub>3</sub> and b) H and other species.

and isolated H atoms are shown respectively. We chose BH<sub>3</sub> as stable species and H as active species. The correlations between stable species with BH<sub>3</sub>, and active species with H were analyzed extensively. From the visualization, we see the predicted data, using the linear correlation, is in good agreement with the actual simulated data. The linear regression models to predict the amount of BH<sub>3</sub> and H radicals are as follow:

BH<sub>3</sub> = 11.7366 \* BCH3 + 20.0063 \* CH4 + 0.1096 \* H2 - 49.3468

H = 2.0213 \* BH + 17.4759 \* BCH + 5.0039 \* CH - 12.5918Table 2 shows a summary of the statistical outcomes of the regression models.

Table 2. Summary of the statistical results of the regression models of BH<sub>3</sub> and H.

	$\mathrm{BH}_3$	Н
Correlation coefficient	0.9973	0.9829
Mean absolute error	29.9541	63.3077
Root mean squared error	37.6899	88.2203
Relative absolute error	7.0828 %	16.4128 %
Root relative squared error	7.35 %	18.4091 %
Total Number of Instances	10100	10100

If we look carefully to the regression model and the summary in the table, stable species BH<sub>3</sub> is highly correlated with other stable species. More importantly, this correlation is linear. Similarly, active isolated hydrogen atoms are linearly correlated with other active species like BH, CH, and BCH. Other correlations can be found from the available data. It should be noted that there can be other species not specified here which might not be significant individually but altogether could have a nontrivial impact. Further detailed study will be needed using larger simulation scales. Nevertheless, these types of correlations might be useful to deduce some of the unmeasurable (low count) species based of the quantity of the measurable species.

Overall, our systematic modeling study confirms some of the observations obtained experimentally.[32] For example, the previous experimental results did indicate that when the percentage of hydrogen content is relatively high, the density is normally low and vice versa.[79,87]. Additionally, we have also been able to show the evolution of the radical or stable species as a function of the Ar bombardment. These modeling results are useful for further strategizing the synthesis process so as to maximize the density and quality of the boron carbide thin films.

# Conclusion

We have successfully modeled the argon bombardment process of *ortho*-carborane using a reactive force field (ReaxFF) molecular dynamics simulation. By varying the energy of argon atoms, we systematically determined the

amount of hydrogen gas and various types of gas species produced. The time evolution of PDF analysis allowed us to monitor the decomposition of *ortho*-carborane molecules as a result of bombardment. In addition, we have successfully identified the dynamics in the free radical formation.

# **Acknowledgments**

We are grateful for the support of NSF (DMREF) Grant no 1729176. The computational work was performed at the National Energy Research Scientific Computing Center (NERSC) under ERCAP0007777 computational project.

## References

- [1] Thévenot F 1990 Boron carbide-A comprehensive review J. Eur. Ceram. Soc.
- [2] Suri A K, Subramanian C, Sonber J K and Murthy T S R C 2010 Synthesis and consolidation of boron carbide: a review *Int. Mater. Rev.* 55 4–40
- [3] Casady J B and Johnson R W 1996 Status of silicon carbide (SiC) as a wide-bandgap semiconductor for hightemperature applications: A review Solid. State. Electron. 39 1409–22
- [4] Tairov Y M and Tsvetkov V F 1978 Investigation of growth processes of ingots of silicon carbide single crystals J. Cryst. Growth 43 209–12
- [5] Begand S, Oberbach T and Glien W 2005 Investigations of the Mechanical Properties of an Alumina Toughened Zirconia Ceramic for an Application in Joint Prostheses Key Eng. Mater. 284–286 1019–22
- [6] Silva M V., Stainer D, Al-Qureshi H A, Montedo O R K and Hotza D 2014 Alumina-Based Ceramics for Armor Application: Mechanical Characterization and Ballistic Testing J. Ceram. 2014 1–6
- [7] Caruso A N, Dowben P A, Balkir S, Schemm N, Osberg K, Fairchild R W, Flores O B, Balaz S, Harken A D and Robertson B W 2006 The all boron carbide diode neutron detector: Comparison with theory *Mater. Sci. Eng. B* 135 129–33
- [8] Bose D K, Nair K U and Gupta C K 1986 Production of high purity boron carbide *High Temp. Mater. Process.* 7 133–40
- [9] Emin D and Aselage T L 2005 A proposed boron-carbidebased solid-state neutron detector J. Appl. Phys. 97 13529
- [10] Robertson B W, Adenwalla S, Harken A, Welsch P, Brand J I, Dowben P A and Claassen J P 2002 A class of boronrich solid-state neutron detectors *Appl. Phys. Lett.* **80** 3644–6
- [11] Sondur R 2001 (12) United States Patent Method Implement. Using Comput. Topol. Objects Pat. No. US 6,352,921 B1 1
- [12] Keski-Kuha R A M, Blumenstock G M, Fleetwood C M and Schmitt D-R 1998 Effects of space exposure on ionbeam-deposited silicon-carbide and boron-carbide coatings Appl. Opt. 37 8038–42
- [13] Hu H and Kong J 2014 Improved thermal performance of diamond-copper composites with boron carbide coating *J. Mater. Eng. Perform.* **23** 651–7
- [14] Chen Y, Chung Y-W and Li S-Y 2006 Boron carbide and boron carbonitride thin films as protective coatings in ultra-high density hard disk drives *Surf. Coatings Technol.*

#### **200** 4072–7

- [15] Vepřek S 1992 Large-area boron carbide protective coatings for controlled thermonuclear research prepared byin situ plasma CVD Plasma Chem. Plasma Process. 12 219–35
- [16] Hayun S, Kalabukhov S, Ezersky V, Dariel M P and Frage N 2010 Microstructural characterization of spark plasma sintered boron carbide ceramics *Ceram. Int.* **36** 451–7
- [17] Zorzi J E, Perottoni C A and da Jornada J A H 2005 Hardness and wear resistance of B4C ceramics prepared with several additives *Mater. Lett.* **59** 2932–5
- [18] Chen M W, McCauley J W, LaSalvia J C and Hemker K J 2005 Microstructural Characterization of Commercial Hot-Pressed Boron Carbide Ceramics J. Am. Ceram. Soc. 88 1935–42
- [19] Bandyopadhyay A K, Beuneu F, Zuppiroli L and Beauvy M 1984 The role of free carbon in the transport and magnetic properties of boron carbide J. Phys. Chem. Solids 45 207–14
- [20] Wood C and Emin D 1984 Conduction mechanism in boron carbide *Phys. Rev. B* **29** 4582
- [21] Lee S, Mazurowski J, Ramseyer G and Dowben P A 1992 Characterization of boron carbide thin films fabricated by plasma enhanced chemical vapor deposition from boranes J. Appl. Phys. 72 4925–33
- [22] Blumenstock G M and Keski-Kuha R A M 1994 Ionbeam-deposited boron carbide coatings for the extreme ultraviolet *Appl. Opt.* **33** 5962–3
- [23] Sezer A O and Brand J I 2001 Chemical vapor deposition of boron carbide Mater. Sci. Eng. B 79 191–202
- [24] Suematsu H, Kitajima K, Suzuki T, Jiang W, Yatsui K, Kurashima K and Bando Y 2002 Preparation of polycrystalline boron carbide thin films at room temperature by pulsed ion-beam evaporation *Appl. Phys. Lett.* 80 1153–5
- [25] Sasaki S, Takeda M, Yokoyama K, Miura T, Suzuki T, Suematsu H, Jiang W and Yatsui K 2005 Thermoelectric properties of boron-carbide thin film and thin film based thermoelectric device fabricated by intense-pulsed ion beam evaporation Sci. Technol. Adv. Mater. 6 181
- [26] Billa R B, Hofmann T, Schubert M and Robertson B W 2009 Annealing effects on the optical properties of semiconducting boron carbide J. Appl. Phys. 106 033515
- [27] Alimov V K, Bogomolov D B, Churaeva M N, Gorodetsky A E, Kanashenko S L, Kanaev A I, Rybakov S Y, Sharapov V M, Zakharov A P, Zalavutdinov R K, Buzhinsky O I, Chernobay A P, Grashin S A, Mirnov S V, Bregadze V I and Usyatinsky A Y 1992 Characterization of a-B/C: H films deposited from different boron containing precursors J. Nucl. Mater. 196–198 670–5
- [28] Sharapov V M, Mirnov S V, Grashin S A, Lebedev S V, Kovan I A, Krasilnikov A V, Krupin V A, Levin L S, Romannikov A N and Zakharov A P 1995 Boronization of Russian tokamaks from carborane precursors J. Nucl. Mater. 220 730–5
- [29] Zhang D, McIlroy D N, O'Brien W L and De Stasio G 1998 The chemical and morphological properties of boron–carbon alloys grown by plasma-enhanced chemical vapour deposition *J. Mater. Sci.* 33 4911–5
- [30] Caruso A N, Billa R B, Balaz S, Brand J I and Dowben P A 2004 The heteroisomeric diode J. Phys. Condens. Matter 16 L139
- [31] Schulz D L, Lutfurakhmanov A, Mayo B, Sandstrom J, Bunzow D, Qadri S B, Bao R, Chrisey D B and Caruso A

- N 2008 Characterization of a-B5C: H prepared by PECVD of orthocarborane: Results of preliminary FTIR and nuclear reaction analysis studies *J. Non. Cryst. Solids* **354** 2369–71
- [32] Nordell B J, Karki S, Nguyen T D, Rulis P, Caruso A N, Purohit S S, Li H, King S W, Dutta D, Gidley D, Lanford W A and Paquette M M 2015 The influence of hydrogen on the chemical, mechanical, optical/electronic, and electrical transport properties of amorphous hydrogenated boron carbide J. Appl. Phys. 118 23–5
- [33] Gamba Z and Powell B M 1996 The condensed phases of carboranes *J. Chem. Phys.* **105** 2436–40
- [34] Thiel W 2009 QM/MM methodology: Fundamentals, scope, and limitations *Multiscale Simul. methods Mol. Sci.* **42** 203–14
- [35] Carter E A 2008 Challenges in modeling materials properties without experimental input. *Science* **321** 800–3
- [36] Cohen A J, Mori-Sánchez P and Yang W 2012 Challenges for Density Functional Theory Chem. Rev. 112 289–320
- [37] Schuch N and Verstraete F 2009 Computational complexity of interacting electrons and fundamental limitations of density functional theory *Nat. Phys.* **5** 732–5
- [38] Van Duin A C T, Dasgupta S, Lorant F and Goddard W A 2001 ReaxFF: a reactive force field for hydrocarbons J. Phys. Chem. A 105 9396–409
- [39] Senftle T P, Hong S, Islam M M, Kylasa S B, Zheng Y, Shin Y K, Junkermeier C, Engel-Herbert R, Janik M J and Aktulga H M 2016 The ReaxFF reactive force-field: development, applications and future directions npj Comput. Mater. 2 15011
- [40] Buehler M J, Tang H, Van Duin A C T and Goddard W A 2007 Threshold crack speed controls dynamical fracture of silicon single crystals *Phys. Rev. Lett.*
- [41] Chenoweth K, Van Duin A C T and Goddard W A 2008 ReaxFF reactive force field for molecular dynamics simulations of hydrocarbon oxidation *J. Phys. Chem. A* 112 1040–53
- [42] Buehler M J, Van Duin A C T and Goddard W A 2006 Multiparadigm modeling of dynamical crack propagation in silicon using a reactive force field *Phys. Rev. Lett.*
- [43] Chenoweth K, Van Duin A C T, Dasgupta S and Goddard W A 2009 Initiation mechanisms and kinetics of pyrolysis and combustion of JP-10 hydrocarbon jet fuel *J. Phys. Chem. A*
- [44] An Q and Goddard III W A 2015 Atomistic origin of brittle failure of boron carbide from large-scale reactive dynamics simulations: suggestions toward improved ductility *Phys. Rev. Lett.* 115 105501
- [45] Neyts E C, Ostrikov K, Han Z J, Kumar S, Van Duin A C T and Bogaerts A 2013 Defect healing and enhanced nucleation of carbon nanotubes by low-energy ion bombardment *Phys. Rev. Lett.* 110 1–5
- [46] Inui N, Mochiji K and Moritani K 2008 Actuation of a suspended nano-graphene sheet by impact with an argon cluster *Nanotechnology* 19
- [47] Baowan, D; Hill J 2007 Nested boron nitride and carbonboron nitride nanocones *Micro Nano Lett.* **2** 67–71
- [48] Křenek P 2008 Thermophysical properties of H 2O-Ar plasmas at temperatures 400-50,000 K and pressure 0.1 MPa Plasma Chem. Plasma Process. 28 107–22
- [49] Lorentz H A 1881 Ueber die Anwendung des Satzes vom Virial in der kinetischen Theorie der Gase *Ann. Phys.*
- [50] Berthelot M P E 1894 Sur l'alteration lente des objects de cuivre, au sein de la terre et dans les musées *Comptes*

- Rendus Hebdomadaires des Séances de l'Academie des
- [51] Plimpton S, Crozier P and Thompson A 2007 LAMMPSlarge-scale atomic/molecular massively parallel simulator Sandia Natl. Lab. 18 43
- [52] Olmsted D L, Foiles S M and Holm E A 2009 Survey of computed grain boundary properties in face-centered cubic metals: I. Grain boundary energy *Acta Mater.* 57 3694–703
- [53] Suter J L, Groen D and Coveney P V. 2015 Chemically Specific Multiscale Modeling of Clay-Polymer Nanocomposites Reveals Intercalation Dynamics, Tactoid Self-Assembly and Emergent Materials Properties Adv. Mater. 27 966–84
- [54] Liyanage L S I, Kim S-G, Houze J, Kim S, Tschopp M A, Baskes M I and Horstemeyer M F 2014 Structural, elastic, and thermal properties of cementite (Fe 3 C) calculated using a modified embedded atom method *Phys. Rev. B* 89 094102
- [55] Hsu D D, Xia W, Arturo S G and Keten S 2014 Systematic Method for Thermomechanically Consistent Coarse-Graining: A Universal Model for Methacrylate-Based Polymers J. Chem. Theory Comput. 10 2514–27
- [56] H. Chris. Greenwell †, Matthew J. Harvey †, Pascal Boulet †, Allen A. Bowden ‡, Peter V. Coveney, \* A and Whiting‡ A 2005 Interlayer Structure and Bonding in Nonswelling Primary Amine Intercalated Clays
- [57] Ratanaphan S, Olmsted D L, Bulatov V V., Holm E A, Rollett A D and Rohrer G S 2015 Grain boundary energies in body-centered cubic metals *Acta Mater.* **88** 346–54
- [58] James L. Suter, Peter V. Coveney \*, H. Chris Greenwell ‡ and and Thyveetil M-A 2007 Large-Scale Molecular Dynamics Study of Montmorillonite Clay: Emergence of Undulatory Fluctuations and Determination of Material Properties
- [59] Kresse G and Furthmüller J 1996 Software VASP, vienna (1999) Phys. Rev. B 54 169
- [60] Kresse G and Joubert D 1999 From ultrasoft pseudopotentials to the projector augmented-wave method Phys. Rev. B 59 1758–75
- [61] Kresse G and Furthmüller J 1996 Efficient iterative schemes for ab initio total-energy calculations using a plane-wave basis set *Phys. Rev. B* **54** 11169–86
- [62] Kresse G and Furthmüller J 1996 Efficiency of ab-initio total energy calculations for metals and semiconductors using a plane-wave basis set *Comput. Mater. Sci.* 6 15–50
- [63] Monkhorst H J and Pack J D 1976 Special points for Brillouin-zone integrations *Phys. Rev. B* 13 5188
- [64] Martinez L, Andrade R, Birgin E G and Martínez J M 2009 PACKMOL: A package for building initial configurations for molecular dynamics simulations J. Comput. Chem.
- [65] Georgieva V, Bogaerts A and Gijbels R 2004 Numerical investigation of ion-energy-distribution functions in single and dual frequency capacitively coupled plasma reactors *Phys. Rev. E - Stat. Nonlinear, Soft Matter Phys.* 69 1–11
- [66] Wu A C F, Lieberman M A and Verboncoeur J P 2007 A method for computing ion energy distributions for multifrequency capacitive discharges
- [67] Jensen B D, Bandyopadhyay A, Wise K E and Odegard G M 2012 Parametric study of ReaxFF simulation parameters for molecular dynamics modeling of reactive carbon gases J. Chem. Theory Comput. 8 3003–8
- [68] Hall M, Frank E, Holmes G, Pfahringer B, Reutemann P and Witten I H 2009 The WEKA data mining software: an

- update ACM SIGKDD Explor. Newsl. 11 10-8
- [69] Frank E, Hall M, Holmes G, Kirkby R, Pfahringer B, Witten I H and Trigg L 2009 Weka-a machine learning workbench for data mining *Data mining and knowledge* discovery handbook (Springer) pp 1269–77
- [70] Markov Z and Russell I 2006 An introduction to the WEKA data mining system ACM SIGCSE Bulletin vol 38 (ACM) pp 367–8
- [71] Witten I H, Frank E, Hall M A and Pal C J 2016 Data Mining: Practical machine learning tools and techniques (Morgan Kaufmann)
- [72] Frank E, Hall M, Trigg L, Holmes G and Witten I H 2004 Data mining in bioinformatics using Weka *Bioinformatics* 20 2479–81
- [73] Garabedian M E and Benson S W 1964 The Kinetics of the Decomposition of BH3CO and the Bond Dissociation Energy of B2H6 J. Am. Chem. Soc. **86** 176–82
- [74] Burg A B and Schlesinger H I 1937 Hydrides of Boron. VII. evidence of the transitory existence of Borine (BH3): Borine Carbonyl and Borine Trimethylammine *J. Am. Chem. Soc.* **59** 780–7
- [75] Wirth H E and Palmer E D 1956 Vapor pressure and dielectric constant of diborane *J. Phys. Chem.* **60** 911–3
- [76] Baughman R H 1970 NMR, calorimetric, and diffraction study of molecular motion in crystalline carboranes *J. Chem. Phys.* **53** 3781–9
- [77] Kawaguchi K 1992 Fourier transform infrared spectroscopy of the BH3v3band *J. Chem. Phys.*
- [78] Imam M, Höglund C, Jensen J, Schmidt S, Ivanov I G,
  Hall-Wilton R, Birch J and Pedersen H 2016
  Trimethylboron as Single-Source Precursor for Boron–
  Carbon Thin Film Synthesis by Plasma Chemical Vapor
  Deposition J. Phys. Chem. C 120 21990–7
- [79] Imam M, Höglund C, Schmidt S, Hall-Wilton R, Birch J and Pedersen H 2018 Plasma CVD of hydrogenated boroncarbon thin films from triethylboron J. Chem. Phys. 148 34701
- [80] Imam M, Gaul K, Stegmüller A, Höglund C, Jensen J, Hultman L, Birch J, Tonner R and Pedersen H 2015 Gas phase chemical vapor deposition chemistry of triethylboron probed by boron–carbon thin film deposition and quantum chemical calculations J. Mater. Chem. C 3 10898–906
- [81] Paquette M M, Li W, Driver M S, Karki S, Caruso A N and Oyler N A 2011 The local physical structure of amorphous hydrogenated boron carbide: insights from magic angle spinning solid-state NMR spectroscopy J. Phys. Condens. Matter 23 435002
- [82] Anan'ev A S, Kon'kov O I, Lebedev V M, Novokhatski A N, Terukov E I and Trapeznikova I N 2002 Fabrication and properties of amorphous hydrogenated boron carbide films Semiconductors 36 941–3
- [83] James R, Pasquale F L and Kelber J A 2013 Plasmaenhanced chemical vapor deposition ofortho-carborane: structural insights and interaction with Cu overlayers J. Phys. Condens. Matter 25 355004
- [84] Bao R, Chrisey D B and Cherniak D J 2011 Kinetics of hydrogen in preparing amorphous B5C:H thin films J. Mater. Res. 26 867–73
- [85] Dong B, Oyelade A and Kelber J A 2017 Carborane-based polymers: a novel class of semiconductors with tunable properties *Phys. Chem. Chem. Phys.* 19 10986–97
- [86] Braddock-Wilking J, Lin S-H and Feldman B J 1998 13 C NMR spectroscopy of amorphous hydrogenated carbon and amorphous hydrogenated boron carbide MRS Online

- Proc. Libr. Arch. 555
- [87] Nordell B J, Keck C L, Nguyen T D, Caruso A N, Purohit S S, Lanford W A, Dutta D, Gidley D, Henry P and King S W 2016 Tuning the properties of a complex disordered material: Full factorial investigation of PECVD-grown amorphous hydrogenated boron carbide *Mater. Chem. Phys.* 173 268–84
- [88] Nordell B J, Nguyen T D, Caruso A N, Purohit S S, Oyler N A, Lanford W A, Gidley D W, Gaskins J T, Hopkins P E, Henry P, King S W and Paquette M M 2017 Carbon-Enriched Amorphous Hydrogenated Boron Carbide Films for Very-Low-k Interlayer Dielectrics Adv. Electron. Mater. 3 1700116
- [89] Belhadj-Larbi M, Horn R C and Rulis P 2017 Model creation and electronic structure calculation of amorphous hydrogenated boron carbide: A classical/: Ab initio hybrid approach *RSC Adv.* **7** 46788–95